Automatic identification of biological microorganisms using three-dimensional complex morphology

Seokwon Yeom
Bahram Javidi
University of Connecticut
Electrical and Computer Engineering Department
371 Fairfield Road, Unit 2157
Storrs, Connecticut 06269-2157
E-mail: Bahram@engr.uconn.edu

Abstract. We propose automated identification of microorganisms using three-dimensional (3-D) complex morphology. This 3-D complex morphology pattern includes the complex amplitude (magnitude and phase) of computationally reconstructed holographic images at arbitrary depths. Microscope-based single-exposure on-line (SEOL) digital holography records and reconstructs holographic images of the biological microorganisms. The 3-D automatic recognition is processed by segmentation, feature extraction by Gabor-based wavelets, automatic feature vector selection by graph matching, training rules, and a decision process. Graph matching combined with Gabor feature vectors measures the similarity of complex geometrical shapes between a reference microorganism and unknown biological samples. Automatic selection of the training data is proposed to achieve a fully automatic recognition system. Preliminary experimental results are presented for 3-D image recognition of *Sphacelaria* alga and *Tribonema aequale* alga. [DOI: 10.1117/1.2187017]

Keywords: microorganism identification; holographic interferometry; three-dimensional image processing; three-dimensional pattern recognition and classification; feature extraction by Gabor-based wavelets.

Paper 05248R received Aug. 24, 2005; revised manuscript received Nov. 22, 2005; accepted for publication Dec. 2, 2005; published online Mar. 24, 2006.

1 Introduction

Three-dimensional (3-D) as well as two-dimensional (2-D) optical and image processing techniques have been investigated to identify specific objects in unknown scenes.[1–13] Automatic and real-time identification of microorganisms has vast potential for various applications such as detection of biological weapons and harmful diseases, diagnosis of diseases, investigation of food safety, and ecological monitoring. There are conventional methods to identify microorganisms; however, the conventional techniques require time-consuming culturing and biochemical analysis with special skills. Therefore, automated and real-time recognition of microorganisms using 3-D optoelectronic imaging and can be beneficial.

Automated discrimination of living microorganisms in unknown images is very challenging. Tiny biological living objects can have simple and undistinguishable morphologies between different species; and many morphological variants exist in the same class.[14] Research and development in this field have been performed using specific color and shapes based on captured 2-D intensity images.[15–20] The identification of tuberculosis bacteria and *Vibrio cholerae* has been studied based on their colors and 2-D shapes.[15,16] In Ref. 17, bacteria in a wastewater treatment plant are identified by morphological descriptors. The aggregation of streptomyces is classified into different phases by measuring the aggregation size and reaction time.[18] In Ref. 19, plankton recognition is performed using preselected geometrical features. More research on image analysis and recognition of microorganisms can be found in Ref. 20. Recently, 3-D microorganism recognition was proposed using the single-exposure on-line (SEOL) digital holography.[3,13]

In this paper, complex information (magnitudes and phase) is utilized, providing distinct features that are impossible to be observed on 2-D intensity images. The phase change is due to the retardation of light as it propagates through the biological sample. We propose the automatic selection process of training data and present experimental results on the recognition of microorganisms. Figure 1 shows the block diagram of the recognition system. Microorganism in the Fresnel diffraction field is recorded by SEOL digital holography.[11–13] Complex amplitude holographic images[21–24] are reconstructed at arbitrary depths by the inverse Fresnel transformation. The complex morphological pattern is segmented and salient features are extracted by the Gabor-based wavelets.[25,26] The training data is automatically selected by means of Gabor feature vectors and the graph matching technique.[27–31] The automatic selection of training data is useful when biological samples overlap and/or cluster, which make it difficult to select individual objects as training data. The rigid graph matching (RGM) techniques measures the similarity of complex geometrical shapes between a reference microorganism and unknown biological objects. A training rule is applied and the mean vector is stored into the database for the known refer-

Address all correspondence to Baram Javidi, Electrical and Computer Engineering Dept., Univ. of Connecticut, 371 Fairfield Road, Unit 2157, Storrs, CT 06269–2157. Tel: 860–486–2867. Fax: 860–486–2447. E-mail: Bahram@engr.uconn.edu

1083-3668/2006/11(2)/024017/8/$22.00 © 2006 SPIE

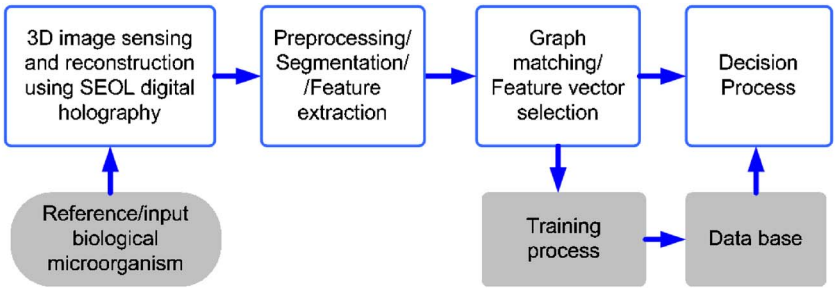

Fig. 1 Block diagram of the automatic and real-time identification system.

ence. For the identification of unknown inputs, Euclidean distance between the reference mean vector and the feature vector of input objects are compared with a threshold.

Section 2 briefly reviews the recording and reconstruction of the SEOL digital holography. The segmentation and Gabor-based wavelets are illustrated in Sec. 3. Section 4 describes the feature vector selection with graph matching. Section 5 presents the training and decision processes. The experimental results and conclusions follow in Secs. 6 and 7, respectively.

2 Review of SEOL Digital Holography

In this section, we review the recording and reconstruction of the 3-D complex information. The complex wave in the Fresnel diffraction field is recorded by the microscope-based Mach-Zehnder interferometer [see Fig. 2(a)]. The 3-D complex holographic images are computationally reconstructed by the inverse Fresnel transformation at arbitrary depth (d) [see Fig. 2(b)]. The SEOL digital holography is adopted for its advantages such as real-time detection and robustness to environmental fluctuation.[13] The reconstruction process of the SEOL digital holography is described in Appendix A. Figure 3 shows the magnitude and the phase of the reconstructed holographic image of *Sphacelaria* alga.

3 Segmentation and Feature Extraction

Since the coherent light is scattered by the semitransparent objects, the intensity on the foreground objects is lower than the background field. During the preprocessing, we subtract the background diffraction field in the reconstructed images. The detailed segmentation process is presented in Appendix B.

After the segmentation, features of microorganisms are extracted by the Gabor-based wavelets to generate a node vector at each pixel. Gabor-based wavelets are composed of multioriented and multiscaled Gaussian-form kernels that are suitable for local spectral analysis.[25,26] We define a node vector at the pixel (m,n) as

$$\mathbf{v}(m,n)=\left[\sum_{v=1}^{V}|h_{1v}(m,n)|\cdots\sum_{v=1}^{V}|h_{Uv}(m,n)|\right]^{t}, \tag{1}$$

$$h_{uv}(m,n)=g_{uv}(m,n)*\hat{O}(m,n), \tag{2}$$

where $g_{uv}(\mathbf{x})$ is the Gabor kernel with indices u and v; U and V are the total number of decompositions along the radial and tangential axes, respectively; $\hat{O}$ is the segmented 3-D complex holographic image; $*$ stands for the 2-D convolution operator, and the superscript t denotes transpose. The kernel of the Gabor-based wavelets is presented in Appendix C.

4 Automatic Training Selection Using Graph Matching

In this section, we utilize the graph-matching technique to choose the data for the training process. The graph-matching technique was developed for pattern recognition of distorted objects.[27–31] However, in the case that the image pattern of a reference object cannot be individually observed, or they are clustered as may be the case with some microorganisms, the selection of training data can be a labor-intensive task. In this paper, we achieve the fully automated recognition system by choosing the feature vectors to be trained by means of the RGM technique.

Let R and T be two identical and rigid graphs that are defined as sets of nodes associated in the local area. The graph R and T are placed on the image O_r and the image O_t of the same reference microorganism, respectively. The reference graph R is translated by a fixed translation vector $\mathbf{p}_r$ and rotated by a fixed clock-wise rotation angle θ_r to cover a predetermined a referenced morphology. Therefore, the position vectors of the nodes in the reference graph R are computed as

$$\mathbf{x}_k(\mathbf{p}_r,\theta_r)=\mathbf{A}(\theta_r)(\mathbf{x}_k^o-\mathbf{x}_c^o)+\mathbf{p}_r,\quad k=1,\ldots,K, \tag{3}$$

$$\mathbf{A}(\theta)=\begin{bmatrix}\cos\theta & \sin\theta\\ -\sin\theta & \cos\theta\end{bmatrix}, \tag{4}$$

where $\mathbf{x}_k^o$ is the position of the node k of a primitive graph without any translation and rotation, $\mathbf{x}_c^o$ is the center of the primitive graph, and K is the total number of nodes in the graph. In a similar way, any rigid motion of the training graph T on the image O_t can be described by a translation vector $\mathbf{p}_t$ and a clockwise rotation angle θ_t as

$$\mathbf{x}_k(\mathbf{p}_t,\theta_t)=\mathbf{A}(\theta_t)(\mathbf{x}_k^o-\mathbf{x}_c^o)+\mathbf{p}_t,\quad k=1,\ldots,K, \tag{5}$$

where $\mathbf{x}_k(\mathbf{p}_t,\theta_t)$ is a position vector of the node k in the graph T.

We sequentially search for a similar local morphology with the referenced morphology on the image O_r by translating and rotating the graph T on the image O_t. We choose the node

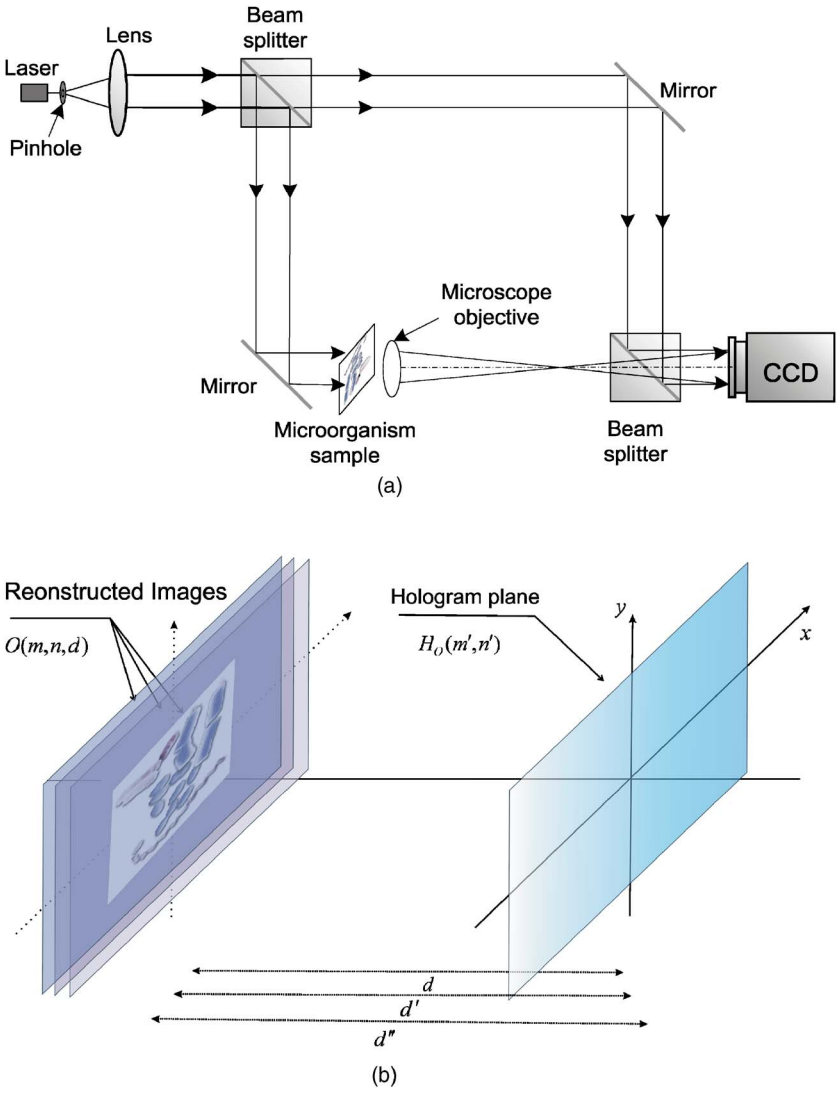

Fig. 2 Schematic diagrams for (a) optical setup of SEOL digital holography and (b) the reconstruction process at arbitrary depth.

vectors $\mathbf{v}_T[\mathbf{x}_k(\mathbf{p}_t, \theta_t)]$ [see. Eq. (1)] of the graph T as training data if the following two conditions are satisfied:

$$S_{RT}(\mathbf{p}_t, \hat{\theta}_t) > \alpha_S \text{ and } C_{RT}(\mathbf{p}_t, \hat{\theta}_t) < \alpha_C, \tag{6}$$

where α_S and α_C are thresholds for the similarity and the difference cost, and $\hat{\theta}_t$ is obtained by searching the best matching angle to maximize the similarity function at the position vector $\mathbf{p}_t$ as

$$\hat{\theta}_t = \arg\max_{\theta_t} S_{RS}(\mathbf{p}_t, \theta_t). \tag{7}$$

The similarity function and the difference cost in Eq. (6) are defined as

$$S_{RT}(\mathbf{p}_t, \theta_t) = \frac{1}{K}\sum_{k=1}^{K} \frac{\langle \mathbf{v}_R[\mathbf{x}_k(\mathbf{p}_r, \theta_r)], \mathbf{v}_T[\mathbf{x}_k(\mathbf{p}_t, \theta_t)]\rangle}{\|\mathbf{v}_R[\mathbf{x}_k(\mathbf{p}_r, \theta_r)]\| \|\mathbf{v}_T[\mathbf{x}_k(\mathbf{p}_t, \theta_t)]\|}, \tag{8}$$

$$C_{RT}(\mathbf{p}_t, \theta_t) = \frac{1}{K}\sum_{k=1}^{K} \|\mathbf{v}_R[\mathbf{x}_k(\mathbf{p}_r, \theta_r)] - \mathbf{v}_T[\mathbf{x}_k(\mathbf{p}_t, \theta_t)]\|, \tag{9}$$

where $\langle\cdot\rangle$ stands for the inner product of two node vectors, and $\mathbf{v}_R[\mathbf{x}_k(\mathbf{p}_r, \theta_r)]$ is the node vector of the graph R.

5 Training and Decision Process

We define a feature vector as the collection of the node vectors of the graph. The feature vector to be trained is presented as

$$\mathbf{f}_T = [\mathbf{v}_T^t[\mathbf{x}_1(\hat{\mathbf{p}}_t, \hat{\theta}_t)] \cdots \mathbf{v}_T^t[\mathbf{x}_K(\hat{\mathbf{p}}_t, \hat{\theta}_t)]]^t, \tag{10}$$

where $\mathbf{v}_T[\mathbf{x}_k(\hat{\mathbf{p}}_t, \hat{\theta}_t)]$ is the node vector of the graph T, which is accepted for training; and the superscript t denotes matrix transpose. One common way for training and testing is to obtain the sample mean of training data and measure the Euclidean distance to determine the identity of unknown inputs. Let a set of training data be Γ:

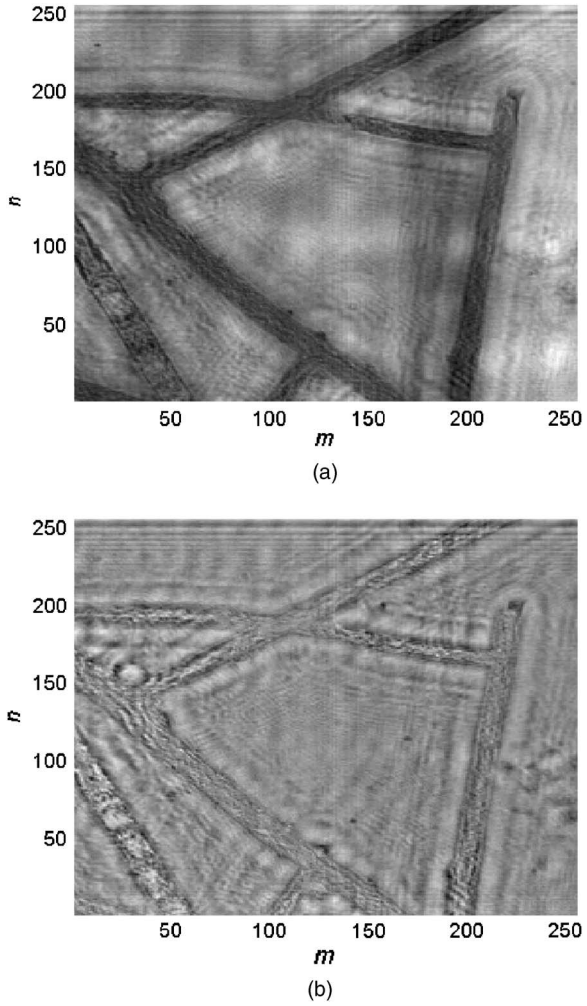

Fig. 3 Computationally reconstructed holographic image of *Sphacelaria* alga (d=180 mm) for (a) magnitude and (b) phase.

$$\Gamma = \{\mathbf{f}_T^1, \ldots, \mathbf{f}_T^{N_T}\}. \tag{11}$$

The set Γ is composed of the feature vectors $\mathbf{f}_T^1, \ldots, \mathbf{f}_T^{N_T}$, where N_T is the total number of the training data. We train those feature vectors by computing the sample mean as

$$\mathbf{m}_f = \frac{1}{N_T} \sum_{i=1}^{N_T} \mathbf{f}_T^i. \tag{12}$$

To recognize unknown inputs, the graph S is translated and rotated on the unknown image O_s as in the training procedure [see Eq. (5)]. The graph S has the same shape and size with the graph R and T. We compare the Euclidean distance with a threshold at every translation vector $\mathbf{p}_s$ and the rotation angle $\hat{\theta}_s$. We accept the detection of the referenced 3-D complex morphology if the following condition is satisfied:

$$\|\mathbf{m}_f - \mathbf{f}_S(\mathbf{p}_s, \hat{\theta}_s)\| < \alpha_D, \tag{13}$$

where α_D is a threshold of detection. The feature vector $\mathbf{f}_S(\mathbf{p}_s, \hat{\theta}_s)$ is obtained from the graph S, which is translated by the vector $\mathbf{p}_s$ and rotated by the angle $\hat{\theta}_s$ as

$$\mathbf{f}_S = [\mathbf{v}_S^t[\mathbf{x}_1(\mathbf{p}_s, \hat{\theta}_s)] \cdots \mathbf{v}_S^t[\mathbf{x}_K(\mathbf{p}_s, \hat{\theta}_s)]]^t, \tag{14}$$

and $\hat{\theta}_s$ is the angle, which minimizes Eq. (13) as

$$\hat{\theta}_s = \min_{\theta_s} \|\mathbf{m}_f - \mathbf{f}_S(\mathbf{p}_s, \theta_s)\|. \tag{15}$$

6 Experimental Results

In the recording of the SEOL digital hologram,[13] the size of the CCD for SEOL digital hologram is 2048×2048 pixels and 1 pixel size is 9×9 μm. The CCD is placed 500 mm from the microorganism samples. The thickness of the microorganisms varies between 10 and 50 μm. To test the recognition performance under various circumstances, we generate SEOL holograms of nine *Sphacelaria* alga and *Tribonema aequale* alga samples, respectively. We denote nine *Sphacelaria* samples as A1,…,A9 and nine *Tribonema aequale* samples as B1,…,B9. Since we have changed the position of the CCD during the experiments to test the robustness of the recognition system, the reconstruction depth for the focused image varies from 180 to 300 mm. After the reconstruction, the magnitude and phase information of computationally reconstructed holographic 3-D images are cropped and reduced into 256-$\times$256-pixel images with a reduction ratio of 0.25 considering the computational complexity.

For the segmentation, we assume less than 20% of lower intensity region is occupied by microorganisms and the intensity of microorganisms is less than 45% of the background diffraction field. Therefore, the maximum intensity rate $r_{\max}$ in Eq. (18) and the segmentation probability P_s in Eq. (19) are set at 0.45 and 0.2, respectively. The parameters for Gabor-based wavelets are set at $\sigma = \pi$, $k_0 = \pi/2$, $\delta = \sqrt{2}$, $U = 5$, and $V = 6$ in Appendix C. Figure 4 shows the component of the node vectors in Eq. (1).

A rectangular grid is selected as a reference graph for the *Sphacelaria* alga, which shows regular thickness (see Fig. 3). The reference graph R is composed of 25×3 nodes and the edge distance between nodes is 4 pixels in the x and y directions. Therefore, the total number of nodes in the graph is 75. The reference graph R is placed with $\mathbf{p}_r = [81, 75]^t$ and $\theta_r = 135$ deg in the sample image A1. Considering the computational load, the graphs T is translated by every 3 pixels in the x and y directions for measuring the similarity and difference to the graph R for the training data selection. To search the best matching angles, the graph T is rotated by 7.5 deg from 0 to 180 deg at every translated location. When the positions of rotated nodes are not integers, they are replaced with the nearest neighbor nodes. For the training data selection, the thresholds α_S and α_C are set at 0.95 and 1.2, respectively, in Eq. (6). For the decision process the threshold α_D is set at 9.5 in Eq. (13). Figure 5(a) shows the reference graph on the sample image A1 and Fig. 5(b) shows automated selection of the training data where 33 graphs (feature vectors) are selected. Figures 5(c) and 5(d) show examples of recognition results performed on the true class sample A3, where 159 feature vectors are identified, and the false class sample B1, where no detection is accepted. Figure 6(a) shows the number of detection in true class samples A1 to A9 and false class samples B1 to B9. The number of detection varies from 14 to

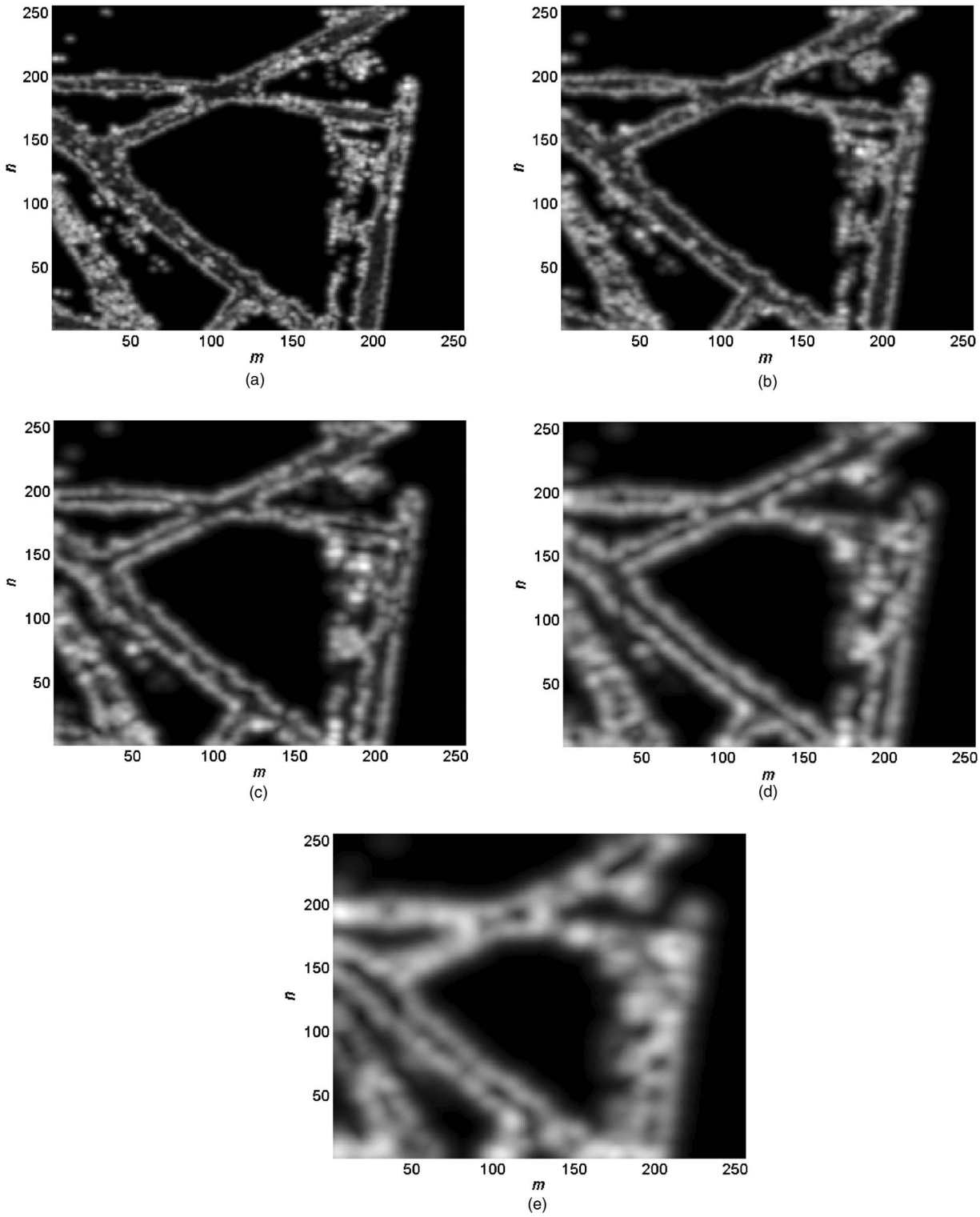

Fig. 4 Components of the node vectors when (a) $u=1$, (b) $u=2$, (c) $u=3$, (d) $u=4$, and (e) $u=5$.

159 in true class samples A1 to A9. No detection is accepted in false class samples B1 to B9. Figure 6(b) shows the minimum Euclidean distance in all samples. The minimum Euclidean distances in false class samples B1 to B9 are larger than those in true class samples A1 to A9 showing the discrimination capability of the proposed recognition system.

7 Conclusions

In this paper, we have described the identification of biological microorganisms using their 3-D complex amplitude of geometrical information obtained by computer-reconstructed SEOL holographic images.[14,32] Segmentation, Gabor feature

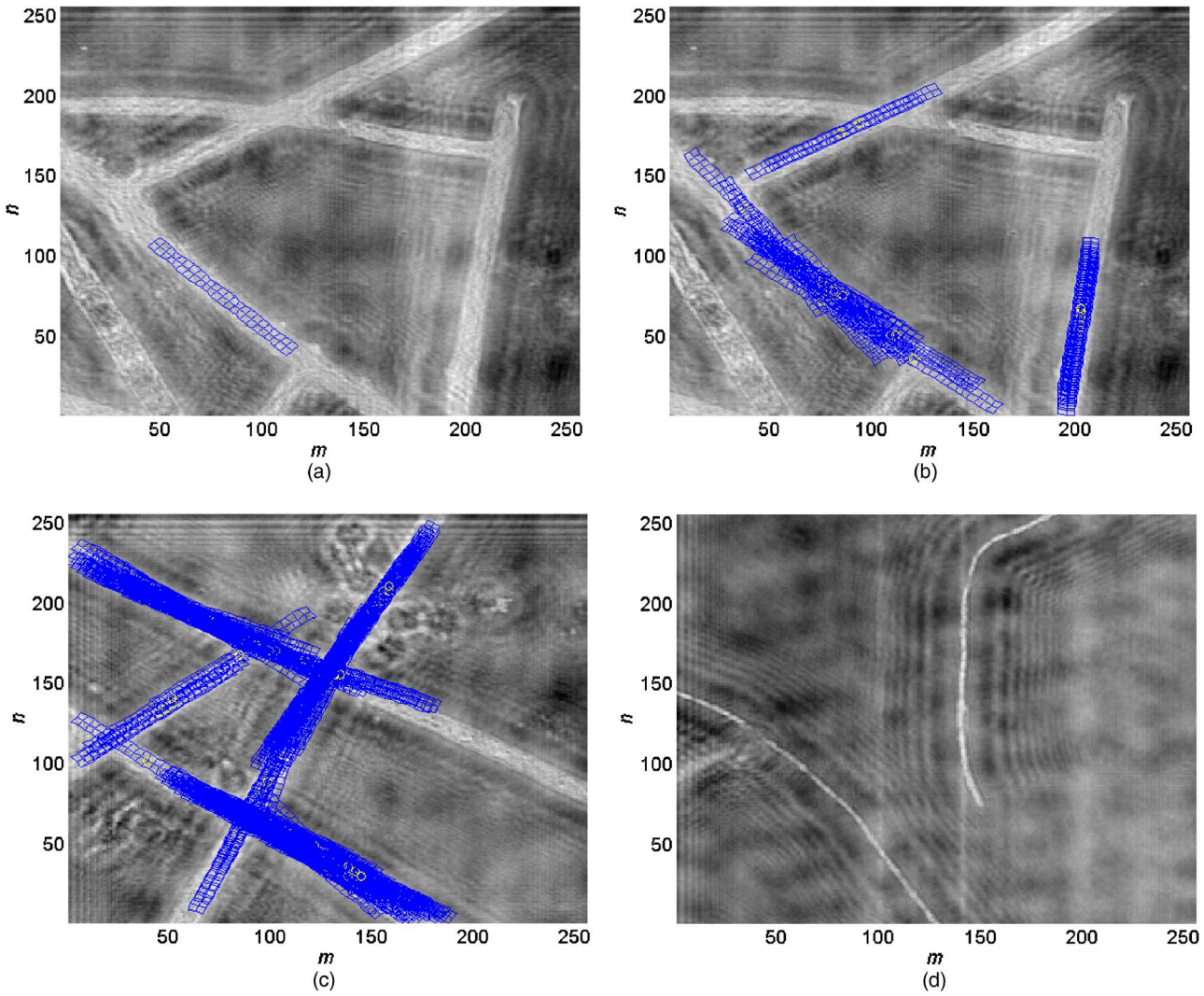

Fig. 5 (a) Reference graph on the sample A1, (b) training data selection on the sample A1, (c) decision result on true class sample A3, and (d) decision result on false class sample B1.

extraction, feature vector selection using graph matching, and training and decision processes are presented to recognize a predetermined 3-D morphology in unknown biological samples. We choose the feature vectors to be trained by means of the RGM technique to remedy the possibility of biological samples overlap and/or cluster, which make it difficult to select individual objects for the training purpose. Training and decision rules are applied to show the performance of the proposed system. Note that more sophisticated training and decision rules can be considered,[7,19] depending on the kind of microorganisms.

Appendix A

The complex Fresnel diffraction field on microorganisms is reconstructed by the inverse Fresnel transformation at 3-D coordinates (m,n,d):

$$O(m,n,d) = \exp\left[-j\frac{\pi}{\lambda d}(\Delta X^2 m^2 + \Delta Y^2 n^2)\right] \times \sum_{m'=1}^{N_x}\sum_{n'=1}^{N_y} H_o(m',n') \times \exp\left[-j\frac{\pi}{\lambda d}(\Delta x^2 m'^2 + \Delta y^2 n'^2)\right] \times \exp\left[j2\pi\left(\frac{mm'}{N_x} + \frac{nn'}{N_y}\right)\right], \quad (16)$$

where $O(m,n,d)$ is the complex amplitude reconstructed at 2-D discrete coordinates (m,n) and depth d; H_o is the SEOL digital hologram; $(\Delta X,\Delta Y)$ and $(\Delta x,\Delta y)$ are 2-D resolutions at the image plane and the hologram plane, respectively; λ is the wavelength of the coherent light source; and N_x and N_y

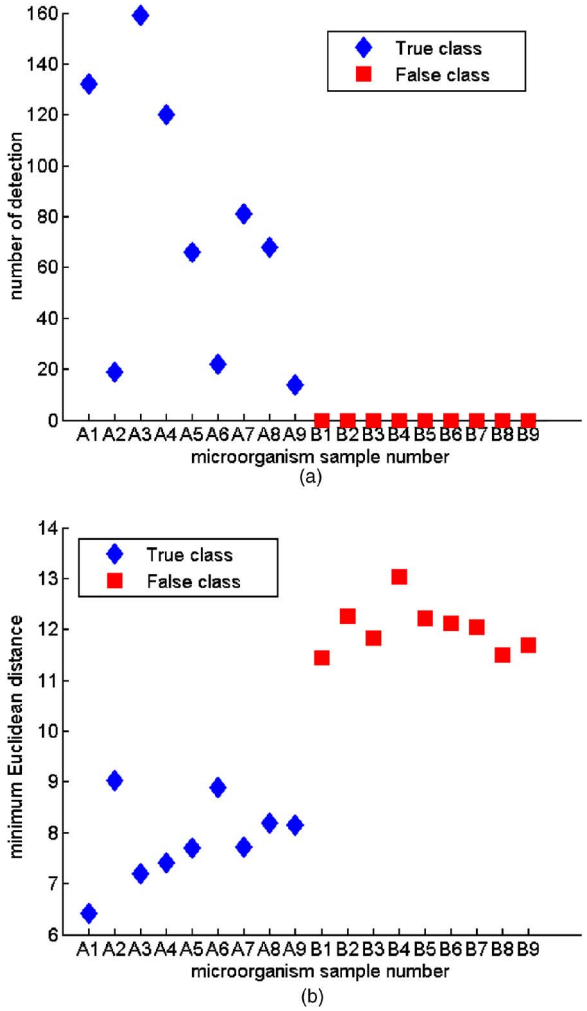

Fig. 6 (a) Number of detections and (b) minimum Euclidean distance.

are the size of the hologram in x and y directions, respectively.

Appendix B

Foreground objects are segmented by means of the histogram analysis of the background diffraction field:

$$\hat{O}(m,n) = \begin{cases} |O(m,n)|\exp\{j[\phi(m,n)-m_\phi]\} & \text{if } |O(m,n)| < I_s \\ 0 & \text{otherwise} \end{cases}, \tag{17}$$

where $O(m,n)$ is the complex holographic image $O(m,n) = |O(m,n)|\exp[j\phi(m,n)]$, and m_ϕ is the sample mean of the phase $\phi(m,n)$.

The threshold I_s is determined from the histogram analysis and the maximum background field:

$$I_s = \min\{\tau_{\kappa_{\min}} r_{\max} \max_{m,n}[|O(m,n)|]\}, \tag{18}$$

where $r_{\max}$ is the maximum rate of the coherent light. The threshold $\tau_{\kappa_{\min}}$ is a minimum value of τ_κ satisfying the following equation:

$$P_s \leqslant \frac{1}{N_x N_y} \sum_{i=1}^{\kappa} h(\tau_i), \tag{19}$$

where P_s is a predetermined segmentation probability; $h(\tau_i)$ is the histogram, i.e., the number of pixels of which magnitude is between τ_{i-1} and τ_i; τ_i is the i'th quantized magnitude level; and $\kappa_{\min}$ is the minimum number of pixels that satisfies Eq. (19). In this paper, the total number of histogram levels is set at 256.

Appendix C

The discrete Gabor kernel $g_{uv}(m,n)$ at the position vector $\mathbf{x} = [m\ n]^t$ is defined as

$$g_{uv}(\mathbf{x}) = \frac{|\mathbf{k}_{uv}|^2}{\sigma^2} \exp\left(-\frac{|\mathbf{k}_{uv}|^2|\mathbf{x}|^2}{2\sigma^2}\right)\left[\exp(j\mathbf{k}_{uv}^t\mathbf{x}) - \exp\left(-\frac{\sigma^2}{2}\right)\right], \tag{20}$$

and the frequency response of the discrete Gabor kernel is

$$G_{uv}(\mathbf{k}) = 2\pi\left\{\exp\left(-\frac{\sigma^2}{2|\mathbf{k}_{uv}|^2}|\mathbf{k}-\mathbf{k}_{uv}|^2\right) - \exp\left[-\frac{\sigma^2}{2|\mathbf{k}_{uv}|^2}(|\mathbf{k}|^2+|\mathbf{k}_{uv}|^2)\right]\right\}, \tag{21}$$

where σ is proportional to the standard deviation of the Gaussian envelope; and $\mathbf{k}_{uv}$ is a discrete wave number vector: $\mathbf{k}_{uv} = k_{0u}[\cos\phi_v\ \sin\phi_v]^t$, $k_{0u} = k_0/\delta^{u-1}$, and $\phi_v = [(v-1)/V]\pi$, where $u = 1,\ldots,U$ and $v = 1,\ldots,V$; k_{0u} is the magnitude of the wave number vector; ϕ_v is the azimuth angle of the wave number vector; k_0 is the maximum carrier frequency of the Gabor kernels; δ is the spacing factor in the frequency domain; u and v are the indices of the Gabor kernels; U and V are the total numbers of decompositions along the radial and tangential axes, respectively.

Acknowledgments

We are grateful to Inkyu Moon for supporting the experiments and the reconstruction on SEOL digital hologram.

References

1. A. K. Jain, *Fundamentals of Digital Image Processing*, Prentice Hall, Englewood Cliffs, NJ (1989).
2. A. Mahalanobis, R. R. Muise, S. R. Stanfill, and A. V. Nevel, "Design and application of quadratic correlation filters for target detection," *IEEE Trans. Aerosp. Electron. Syst.* **40**, 837–850 (2004).
3. B. Javidi, Ed., *Optical Imaging Sensor and Systems for Homeland Security*, Springer, New York (2005).
4. H. Sjoberg, F. Goudail, and P. Refregier, "Optimal algorithms for target location in nonhomogeneous binary images," *J. Opt. Soc. Am. A* **15**, 2976–2985 (1998).
5. H. Kwon and N. M. Nasrabadi, "Kernel RX-algorithm: a nonlinear anomaly detector for hyperspectral imagery," *IEEE Trans. Geosci. Remote Sens.* **43**, 388–397 (2005).

6. F. Sadjadi, Ed., *Selected Papers on Automatic Target Recognition*, SPIE- CDROM (1999).
7. F. Sadjadi, Ed., *Milestones in Performance Evaluations of Signal and Image Processing Systems*, SPIE Press, Bellingham, WA (1993).
8. B. Javidi, Ed., *Image Recognition and Classification: Algorithms, Systems, and Applications*, Marcel Dekker, New York (2002).
9. B. Javidi and F. Okano Eds., *Three-Dimensional Television, Video, and Display Technologies*, Springer, New York (2002).
10. B. Javidi and E. Tajahuerce, "Three dimensional object recognition using digital holography," *Opt. Lett.* **25**, 610–612 (2000).
11. O. Matoba, T. J. Naughton, Y. Frauel, N. Bertaux, and B. Javidi, "Real-time three-dimensional object reconstruction by use of a phase-encoded digital hologram," *Appl. Opt.* **41**, 6187–6192 (2002).
12. B. Javidi and D. Kim, "Three-dimensional-object recognition by use of single-exposure on-axis digital holography," *Opt. Lett.* **30**, 236–238 (2005).
13. D. Kim and B. Javidi, "Distortion-tolerant 3-D object recognition by using single exposure on-axis digital holography," *Opt. Express* **12**, 5539–5548 (2005).
14. B. Javidi, I. Moon, S. Yeom, and E. Carapezza, "Three-dimensional imaging and recognition of microorganism using single-exposure on-line (SEOL) digital holography," *Opt. Express* **13**, 4492–4506 (2005).
15. J. W. Lengeler, G. Drews, and H. G. Schlegel, *Biology of the Prokaryotes*, Blackwell, New York (1999).
16. M. G. Forero, F. Sroubek, and G. Cristobal, "Identification of tuberculosis bacteria based on shape and color," *Real-Time Imag.* **10**, 251–262 (2004).
17. J. Alvarez-Borrego, R. R. Mourino-Perez, G. Cristobal-Perez, and J. L. Pech-Pacheco, "Invariant recognition of polychromatic images of Vibrio cholerae 01," *Opt. Eng.* **41**, 872–833 (2002).
18. A. L. Amaral, M. da Motta, M. N. Pons, H. Vivier, N. Roche, M. Moda, and E. C. Ferreira, "Survey of protozoa and metazoa populations in wastewater treatment plants by image analysis and discriminant analysis," *Environmetrics* **15**, 381–390 (2004).
19. S.-K. Treskatis, V. Orgeldinger, H. Wolf, and E. D. Gilles, "Morphological characterization of filamentous microorganisms in submerged cultures by on-line digital image analysis and pattern recognition," *Biotechnol. Bioeng.* **53**, 191–201 (1997).
20. T. Luo, K. Kramer, D. B. Goldgof, L. O. Hall, S. Samson, A. Remsen, and T. Hopkins, "Recognizing plankton images from the shadow image particle profiling evaluation recorder," *IEEE Trans. Syst. Man Cybern.* **34**, 1753–1762 (2004).
21. J. M. S. Cabral, M. Mota, and J. Tramper, Eds., "Image analysis and multiphase bioreactor," Chap. 2 in *Multiphase Bioreactor Design*, Taylor & Francis, London (2001).
22. J. W. Goodman, *Introduction to Fourier Optics*, 2nd ed., McGraw Hill, Boston (1996).
23. A. Macovski, S. D. Ramsey, and L. F. Schaefer, "Time-lapse interferometry and contouring using television systems," *Appl. Opt.* **10**, 2722–2727 (1971).
24. K. Creath, "Phase-shifting speckle interferometry," *Appl. Opt.* **24**, 3053–3058 (1985).
25. T. Zhang and I. Yamaguchi, "Three-dimensional microscopy with phase-shifting digital holography," *Opt. Lett.* **23**, 1221–1223 (1998).
26. J. G. Daugman, "Uncertainty relation for resolution in space, spatial frequency, and orientation optimized by two-dimensional visual cortical filters," *J. Opt. Soc. Am.* **2**, 1160–1169 (1985).
27. J. G. Daugman, "How iris recognition works," *IEEE Trans. Circuits Syst. Video Technol.* **14**, 21–30 (2004).
28. M. Lades, J. C. Vorbruggen, J. Buhmann, J. Lange, C. V. D. Malsburg, R. P. Wurtz, and W. Konen, "Distortion invariant object recognition in the dynamic link architecture," *IEEE Trans. Comput.* **42**, 300–311 (1993).
29. S. Yeom, B. Javidi, Y. J. Roh, and H. S. Cho, "Three-dimensional object recognition using x-ray imaging," *Opt. Eng.* **44**, 027201 (Feb. 2005).
30. R. P. Wurtz, "Object recognition robust under translations, deformations, and changes in background," *IEEE Trans. Pattern Anal. Mach. Intell.* **19**, 769–775 (1997).
31. B. Duc, S. Fischer, and J. Bigun, "Face authentification with Gabor information on deformable graphs," *IEEE Trans. Image Process.* **8**, 504–516 (1999).
32. S. Yeom, I. Moon, and B. Javidi, "Real-time 3–D sensing, visualization, and recognition of dynamic biological microorganisms," *Proc. IEEE* **94**, 550–566 (2006).